Nano Materials Science 7 (2025) 761–772

Contents lists available at ScienceDirect

Nano Materials Science

journal homepage: www.keaipublishing.com/cn/journals/nano-materials-science/

Exploring Ce(IV)-MOFs redox behavior for catalysis by spectroscopies

Valeria Finelli [a,b], Sergio Rojas-Buzo [a,c,*], Matteo Signorile [a], Francesca Bonino [a], Silvia Bordiga [a,**]

[a] Department of Chemistry, NIS and INSTM Reference Centre, Università di Torino, Via G. Quarello 15/A, I-10135, Via P. Giuria 7, I-10125, Turin, Italy
[b] University School for Advanced Studies, IUSS Pavia, Palazzo del Broletto, Piazza della Vittoria 15, I-27100, Pavia, Italy
[c] Instituto de Tecnología Química, Universitat Politècnica de València - Consejo Superior de Investigaciones Científicas, Av. de los Naranjos, s/n, 46022, Valencia, Spain

ARTICLE INFO

Keywords:
Ce-MOFs
Redox Ce(IV)/Ce(III) pair
Catalysis
Spectroscopy

ABSTRACT

In the Metal-Organic Framework (MOF) panorama, Ce(IV)-based MOFs have emerged as potential candidates for heterogeneous catalysis, not only due to their intrinsic active species but also as a support of single metal sites. As the catalytic behavior of these materials is often associated to the redox properties of cerium, a large number of spectroscopic techniques have been employed to characterize them. Unfortunately, both data acquisition and interpretation are not always straightforward and sometimes the data are not well reported and discussed, limiting their impact in the literature. In this perspective review, we critically analyse the contributions provided by different spectroscopic techniques, sometime supported by molecular modelling approaches, to unravel the nature of Ce(IV)-MOFs at any stage of their preparation and along their use (*i.e.*, post-synthesis treatments and under reaction conditions). A concise description of major results from the recent literature allows to provide basic insights associated to the applicability and limits of most used spectroscopic approaches, showing that more robust understanding of Ce(IV)-MOFs can be achieved when a broad spectrum of techniques are used in parallel, adopting similar conditions and following good practice rules.

1. Introduction

Metal-Organic Frameworks (MOFs) have emerged as versatile porous materials for diverse applications, including heterogeneous catalysis [1–3]. However, one of the main challenging issues for MOFs implementation is their instability under real reaction conditions. In this sense, tetravalent-based MOFs, Zr(IV) and Hf(IV), have demonstrated superior chemical, thermal and mechanical stabilities [4–7]. Moreover, they possess intrinsic features that make them excellent candidates for heterogeneous catalysis: i) presence of both Brønsted and Lewis active sites on the metallic clusters that can serve also to support additional metal units; ii) pore tunability due to the large amount of available organic ligands, that can avoid the formation of non-desired products by steric hindrance; iii) high surface areas that favour mass transport. Ce(IV)-based MOFs are also accessible in the full range of structures as the Zr(IV)-counterparts and recently they have widely gained scientific attention, mainly for their cost-effectiveness and for the good compromise between their redox properties ascribable to valence switching of the Ce(IV)/Ce(III) redox couple [7,8]. Concerning ligands variability for the synthesis of Ce(IV)-based MOFs, one of the most common ligand-to-metal cluster connectivity for these materials is 12, *i.e.*, the one for UiO-66(Ce) [9] and UiO-67(Ce) [10] structures with a ditopic terephthalic acid (H_2BDC) and biphenyl-4,4′-dicarboxylic acid (H_2BPDC) (-based) ligands, respectively. Instead, DUT-67(Ce), [10] obtained using a ditopic 3,5-pyrazole dicarboxylic acid (H_2PZDC) linker, is based on a 8 connectivity. The synthesis of MOF-808(Ce) [10] is carried out using a tritopic benzene-1,3,5-tricarboxylic acid (H_2BTC) linker, and it is based on a 6 connectivity. A tetratopic 1,3,6,8-tetrakis(*p*-benzoic acid)pyrene (H_4TBAPy) linker is used for constructing NU-1000(Ce) [11] structures, exhibiting a 8 connectivity. For instance, if we focus on the UiO-67-type topology, UiO-67(Ce) [10] can be attained with quicker kinetically driven synthetic procedure at milder temperatures with respect to its Zr-counterpart (UiO-67(Zr)), even employing a mixed-linker approach [12], while the thermodynamically favoured material is MIL-140(Ce) [13]. In order to deeply investigate and understand the nature of the active sites in these MOFs, several spectroscopic techniques have been

* Corresponding author. Instituto de Tecnología Química, Universitat Politècnica de València - Consejo Superior de Investigaciones Científicas, Av. de los Naranjos, s/n, 46022, Valencia, Spain.
** Corresponding author.
E-mail addresses: serrobu@upv.edu.es (S. Rojas-Buzo), silvia.bordiga@unito.it (S. Bordiga).

https://doi.org/10.1016/j.nanoms.2024.11.001
Received 26 July 2024; Accepted 24 October 2024
Available online 19 November 2024

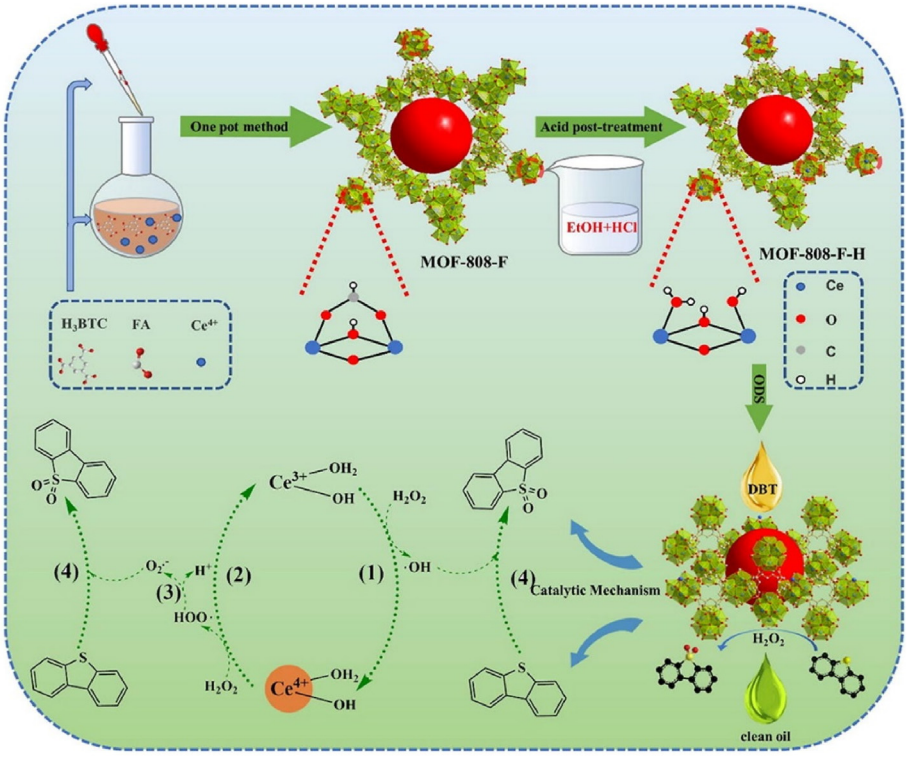

Fig. 1. Synthesis and post-synthetic acid-treatment of Ce-MOF-808, applied for the oxidative desulfurization of DBT, with the corresponding catalytic mechanism. Adapted with permission from Ref. [36]. Copyright 2022 Elsevier.

used bringing mainly qualitative insights, despite its influence in the final catalytic activity that still needs further studies.

Starting from handy characterization techniques, *in situ* infra-red (IR) spectroscopy is useful to monitor solvent removal, hydroxyls population and more in general functional species at the surfaces (both internal and external) [14]. In case of material subjected to post-synthetic treatments, it allows monitoring the changes caused by the appearance of new functional groups [15,16]. The protocols are not very sophisticated "*per se*" but require to be followed with few simple good practice rules. Measurements performed in transmission allow easier normalization in respect to the sample thickness; those carried out on pure samples and in a controlled atmosphere, possibly after solvent removal, allow to monitor the presence of defective species such as extra hydroxyls groups that can be exploited as anchoring site in case of post-synthetic functionalization. Conversely, IR spectra collected in attenuated total reflection (ATR) mode on pure powders or transmission IR spectra collected on halide salt diluted samples are much less informative and sometimes easily bring to oversimplified interpretation of the results [17]. Moreover, IR spectroscopy can become one of the most powerful surface techniques to study high surface area heterogeneous catalysts due to its potential in identifying adsorbate interactions [18]. In particular, the adsorption of probe molecules, such as pyridine [19], deuterated acetonitrile (CD_3CN) [20] and carbon monoxide (CO) [20,21], provides detailed information on the nature of acidic sites. In case of pyridine, a strong basic molecule able to identify the nature of acidic sites (discriminating between Brønsted and Lewis acid sites - BAS and LAS) with different strengths, their quantification is possible by exploiting the knowledge of molar extinction coefficients for the band at 1 455 cm^{-1} (corresponding to the 19b vibrational mode of pyridine adsorbed on LAS) and for the one at 1 545 cm^{-1} (corresponding to the 19b vibrational mode of pyridinium ion adsorbed on BAS) [22]. Unfortunately, in case of MOFs, these fingerprints fall in a region hardly accessible because of the intense carboxylate vibrations [23]. CD_3CN, which is also a relatively strong base, for instance can be used to qualitatively recognize Ce(IV) and Zr(IV) sites even in the absence of open-metal sites [24]. On the other hand, the adsorption of CO, which is facilitated at liquid nitrogen temperature (LNT), guarantees an indirect method for probing qualitatively open-metal sites accessibility, if they have at least one coordination vacancy. Moreover, CO adsorption monitored by IR spectroscopy can also serve to identify Ce(III) sites through the detection of a band at 2 125 cm^{-1} which is ascribed to the CO–Ce(III) adduct [25]. The presence of reduced Ce sites can be also corroborated by other laboratory techniques as diffuse reflectance UV-visible (UV-vis) spectroscopy, electron paramagnetic resonance (EPR) and X-ray photoemission spectroscopy (XPS). The formation of oxygen vacancies, and the consequent Ce(III) increase, could be detected by the red-shift of the absorption edge on the UV-vis spectra of activated MOFs [26]. Moreover, although Ce(III) species are EPR silent due to its low relaxation time [27], its presence could be indirectly revealed by the formation of superoxide O_2^- species, when O_2 reacts on Ce(III) sites [28,29]. Finally, XPS has been also employed to distinguish between Ce(IV) and Ce(III) at the surfaces, even if Ce(III) quantification could be influenced by the analysis conditions themselves [30]. In fact, the high vacuum conditions in the measuring chamber often cause some oxygen loss at the surface and the consequent formation of some extra Ce(III).

In addition, X-ray absorption spectroscopy (XAS), yet still often widely synchrotron radiation based, is a versatile bulk technique for both *in situ* and *operando* evaluations of the oxidation state and the local coordination number of the redox species present in the materials [31]. Even if XAS is an element selective technique, it is important to underline that its result is also element averaged on all the species of the analysed material. In particular, in case of Ce-based materials, there is the possibility to work at K (around 40 keV), L (between 6.5 keV and 5.7 keV) and M (between 1.4 keV and 0.8 keV) edges [32,33]. A niche application in this field is ambient pressure Near Edge X-Ray Absorption Spectroscopy (AP-NEXAFS), a surface technique, that provides information on the oxidation state of Ce without showing the drawback of XPS, that easily causes modifications of the samples during the measurements [34,35].

With the intention to underline their wide possibilities, this perspective review aims at offering a summary of the spectroscopic

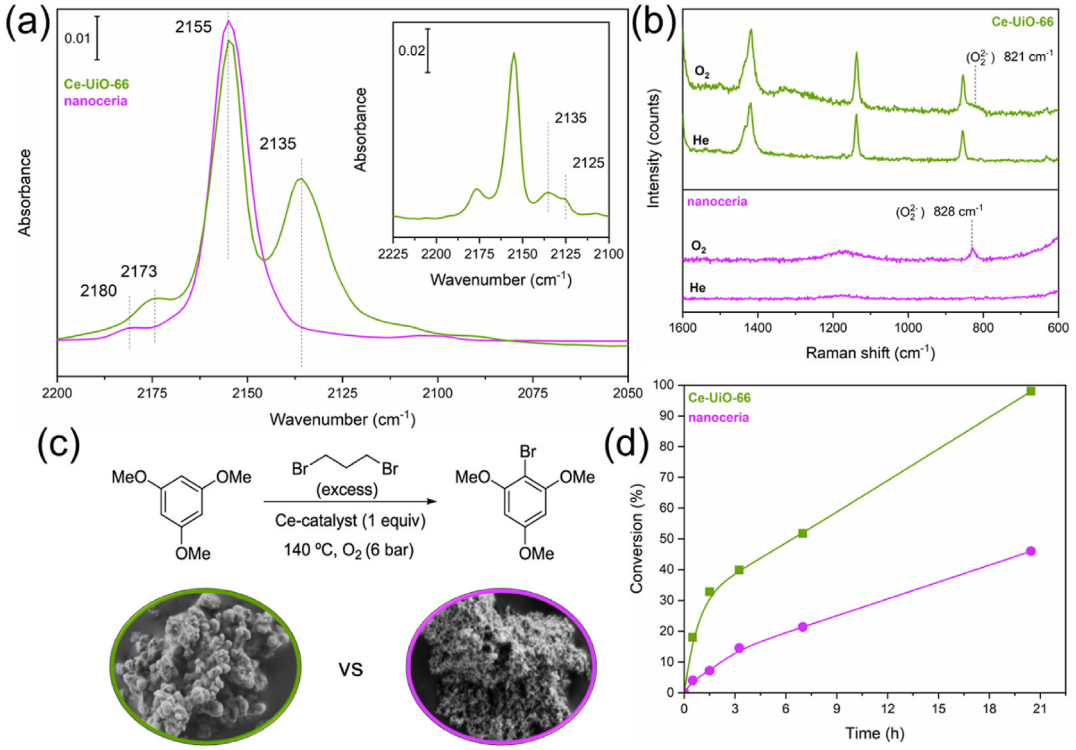

Fig. 2. (a) CO adsorption at LNT monitored by transmission IR spectroscopy at 2 mbar CO coverage for Ce-UiO-66 (green line) and CeO_2 (purple line). 0.5 mbar CO coverage is represented in the inset for Ce-UiO-66; (b) Raman spectra of Ce-UiO-66 and CeO_2 under *in situ* conditions at 140 °C under inert conditions (bottom spectra) and under an oxygen atmosphere (top spectra); (c) Oxidative halogenation of activated TMB with 1,3-dibromopropane as brominating agent and Ce-based materials as catalysts. FESEM images of Ce-UiO-66 and CeO_2 are shown; (d) Kinetic profiles for TMB conversion using Ce-UiO-66 and CeO_2 as catalysts. Adapted with permission from Ref. [25]. Copyright 2021 American Chemical Society.

characterization methods used to study different Ce(IV)-based MOFs with a focus on their catalytic implications. All these spectroscopic characterization methods could disclose insights on materials properties and reaction mechanisms, as discussed in the following sections devoted to both Ce(IV)-MOFs and functionalized Ce(IV)-MOFs and their (photo) catalytic applications.

2. Ce(IV)-MOFs

2.1. *Ce(IV)-MOFs for thermocatalytic applications*

Ce(IV)-MOFs possess weak surface Lewis acidity and a redox chemistry that make them potential candidates for heterogeneous catalysis. For instance, Chu et al. [36] reported that the catalytic activity for the oxidative desulfurization of dibenzothiophene (DBT) is enhanced by the presence of open-metal sites and the redox Ce(IV)/Ce(III) couple. In this sense, defective Ce-MOF-808 (named as MOF-808-F-H) was prepared by treating the as-prepared Ce(IV)-MOF (denoted as MOF-808-F since it was synthesised with formic acid (F) as modulator) with HCl (pH 1.5 for 1 h) leading to open-metal sites by removal of coordinating formic acid (Fig. 1). The number of Ce(III) species increased in the acid-treated sample, as was deduced by XPS spectroscopy (from 36.8 % to 40.4 %). Moreover, the authors used IR spectroscopy in combination with pyridine adsorption, aiming to identify both BAS and LAS species. The approach is interesting as it explores the possibility to use pyridine as a probe molecule, monitoring three bands in the 1 010 cm^{-1} to 1 080 cm^{-1} interval [37]. Unfortunately, the publication does not report a detailed description of the experiment conditions and data treatment, limiting its impact. At last, the authors concluded that the synergism between the higher amount of LAS and the redox activity of MOF-808-F-H is responsible to its enhanced activity in the oxidative desulfurization of DBT. In fact, the reaction mechanism was disclosed to be as an activation of H_2O_2 on defective Ce(III) sites, the effective LAS species, with the generation of reactive oxygen species which promote the complete oxidative desulfurization of DBT after 15 min at 50 °C (Fig. 1).

In a similar way, Dalapati et al. [38] applied XPS spectroscopy to a Ce-UiO-66 for having insights on the catalytic surface sites, corroborating the presence of 23.6 % of Ce(III) species. They claimed that the initial presence of both Ce(III) and Ce(IV) ions makes him an excellent heterogeneous catalyst for the aerobic oxidation of thiols. However, as we anticipated previously in the introduction section, XPS as a single characterization technique to probe the presence of Ce(III) sites offers reproducibility issues and cannot discriminate between accessible and not accessible surface sites, thus complementary spectroscopic techniques should be employed to corroborate its presence. In this sense, Rojas-Buzo et al. [25] probed that CO adsorption at LNT monitored by transmission IR spectroscopy is a powerful tool to identify accessible Ce(III) sites in MOFs by the appearance of the band at 2 125 cm^{-1} associated with Ce(III)-CO adduct (Fig. 2a). Moreover, the authors compared its catalytic activity for the oxidative halogenation of activated arenes with the one obtained with a nanocrystalline cerium oxide (Fig. 2c). The Ce(IV)-MOF showed complete 1,3,5-trimethoxybenzene (TMB) conversion after 21 h while CeO_2 showed only 46 % in the same period (Fig. 2d). Even if the initial presence of Ce(III) species was corroborated by XPS spectroscopy for both samples, IR spectra of adsorbed CO at LNT qualitatively probed the presence of accessible Ce(III) sites on Ce-UiO-66 while this contribution was not detected on cerium oxide, explaining its lower catalytic activity. Finally, the reaction mechanism was unveiled by means of Raman spectroscopy conducted under opportune *in situ* conditions and it follows an analogous pathway than the one reported for metalloenzymes (Fig. 2b): defective Ce(III) site on Ce_6-node activates oxygen by the formation of η^2-peroxy species (O_2^{2-}), which is essential for the generation of the electrophilic intermediate for the synthesis of bromo-arenes [25].

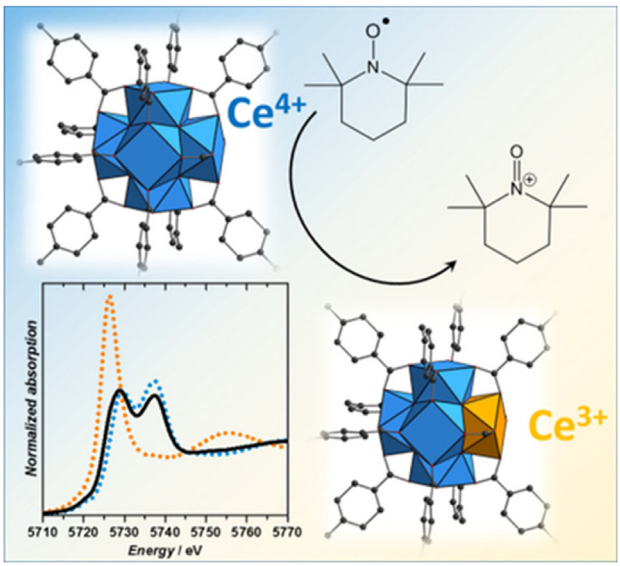

Fig. 3. Ce L_3-edge XANES spectra of Ce-UiO-67 reacted (solid black line), Ce(IV) reference, namely Ce-UiO-66 (dotted blue line) and Ce(III) reference, namely $Ce(NO_3)_3{\cdot}6H_2O$ (dotted orange line). Adapted with permission from Ref. [39]. Copyright 2018 John Wiley and Sons.

As anticipated, apart from XPS, XAS spectroscopies are meaningful for detecting the presence of reduced Ce(III) species. In this sense, a detailed XAS study at both L_3- and K-edges, was conducted by Smolders et al. [39] on Ce-UiO-67, employed as catalyst for 2,2,6,6-tetramethyl-1-piperidinyloxy (TEMPO)-mediated aerobic oxidation of benzyl alcohol. Ce-UiO-66 and $Ce(NO_3)_3{\cdot}6H_2O$ were used as Ce(IV) and Ce(III) references, respectively, for a linear combination fit analysis of both L_3- and K-edges of the Ce-UiO-67 reacted with TEMPO/benzyl alcohol mixture. It revealed that one atom per Ce_6-cluster can be reduced to Ce(III) during the catalytic cycle by a two-electron oxidation process: one electron is provided by the Ce(IV)/Ce(III) redox pair, while TEMPO acts as a redox mediator to compensate the other missing electron, revealing a synergic action (Fig. 3). Moreover, the so-formed Ce(III) species, characterized by a larger ionic radius, does not have any negative effect on the framework stability. Finally, the catalytic activity for the oxidation of benzyl alcohol was compared with the one obtained for other Ce(IV)-based MOFs. Ce-MOF-808, with bigger MOF cavities and lower cluster connectivity than UiO-66 and UiO-67 analogues, exhibited the best catalytic performance.

2.2. Ce(IV)-MOFs for health safety, environment and energy applications

Among pollutants, surely mercury (Hg) is very dangerous, causing permanent damage to kidneys, heart and nervous system also at low concentrations. Focussing on Ce(IV)-MOFs applications in this field, Zhang et al. [40] reported the colorimetric sensing of Hg(II) using an Ce-UiO-66-TMB (3,3′,5,5′-tetramethylbenzydine) framework. Ce-UiO-66 nanoparticles (NPs) were suspended with TMB in an acetate buffer solution, and the mixture was incubated at 35 °C for 10 min for the oxidation of TMB. Upon the reduction of Ce(IV) species of Ce-UiO-66 NPs, which effectively behave as electron mediators, TMB could be oxidised without modifications and combinations with other catalytic components. The peroxidase mimetic feature of Ce-UiO-66 is weakened by the presence of Hg(II), which is chelated by the amino groups of two TMB molecules (Fig. 4a). Based on these data, Zhang et al. reported for the first time the inhibition of TMB oxidation by Hg(II) species by adopting its colorimetric sensing. This trend can be monitored using UV-vis spectroscopy to measure the absorbance intensity of the Ce-UiO-66-TMB system at 652 nm, which corresponds to the blue colour of oxidised TMB. In fact, this intensity is decreased as the concentration of Hg(II) increases (see Fig. 4b). No influence to the absorption intensity at 652 nm was observed by other possible tested cations with ten times higher concentrations (Fig. 4c).

As a variation on the UiO-66(Ce) framework, CSUST-1, a mixed-valence Ce-MOF with isolated Ce(IV)/Ce(III) arrays and abundant oxygen vacancies (Ce(III)-V_O), was prepared by following the simple synthetic route of UiO-66(Ce) while also demonstrating kinetic stability [41]. CSUST-1 could be prepared either by increasing the molar ratio of terephthalic acid (H_2BDC) to metallic Ce precursor to 3:1, which is kept 1:1 for UiO-66(Ce), or by soaking it in a DMF solution of H_2BDC at 120 °C

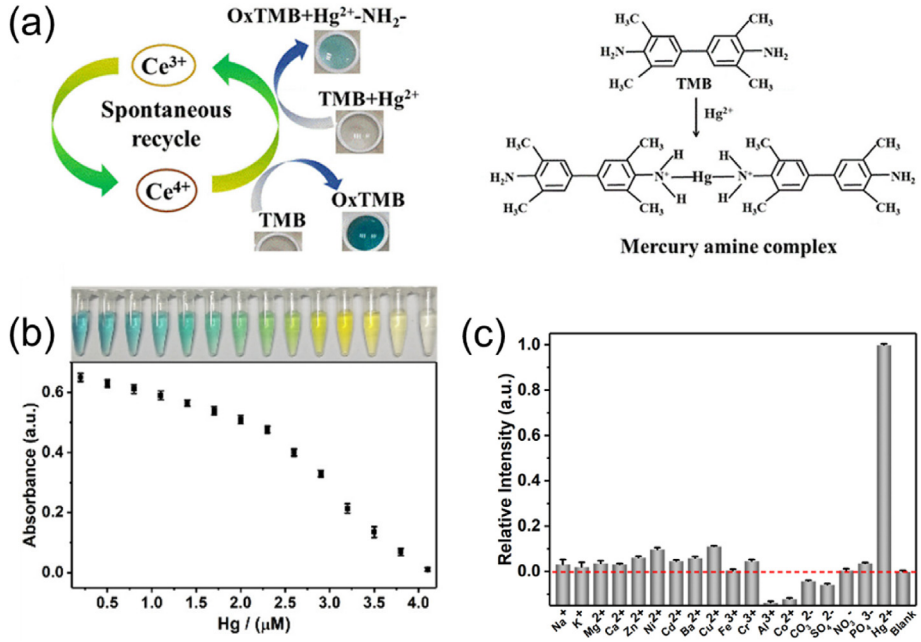

Fig. 4. (a) Colorimetric sensing of Hg(II) using Ce-UiO-66-TMB system; (b) Absorbance intensity at 652 nm of Ce-UiO-66-TMB trend related to the concentration of Hg(II); (c) Relative decrease of absorbance intensity at 652 nm of Ce-UiO-66-TMB with Hg(II) (1.5 μM) and other cations (15 μM). Adapted with permission from Ref. [40]. Copyright 2019 Elsevier.

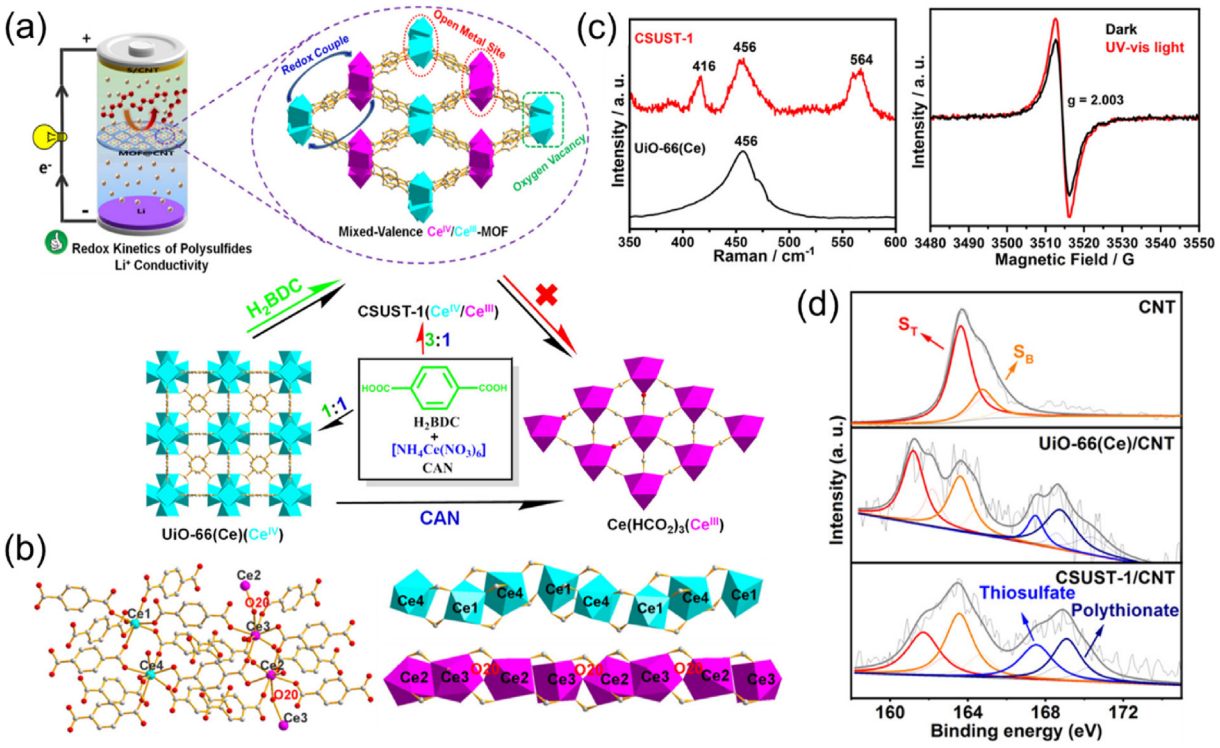

Fig. 5. (a) Synthesis and (b) Framework structure of CSUST-1; (c) Raman spectra of CSUST-1 and UiO-66(Ce) and RT EPR spectra obtained from CSUST-1 in dark and after UV−vis light irradiation; (d) XPS spectra at S 2p region of CNT, UiO-66(Ce)/CNT and CSUST-1/CNT after Li_2S_4 adsorption. Adapted with permission from Ref. [41]. Copyright 2021 American Chemical Society.

for one week (Fig. 5a). As depicted in Fig. 5b, in this structure, Ce(III) and Ce(IV) ions are linked to the terephthalate (BDC^{2-}) ligands to form a one dimensional (1D) Ce(IV) chain, while a 1D Ce(III) chain is resulting from the interconnection of the Ce2 and Ce3 ions sharing an O^{2-} bridge via the carboxylate groups. Raman and EPR spectra confirmed the presence of Ce(III)-V_0 in the CSUST-1 framework (Fig. 5c). In fact, the Raman band at

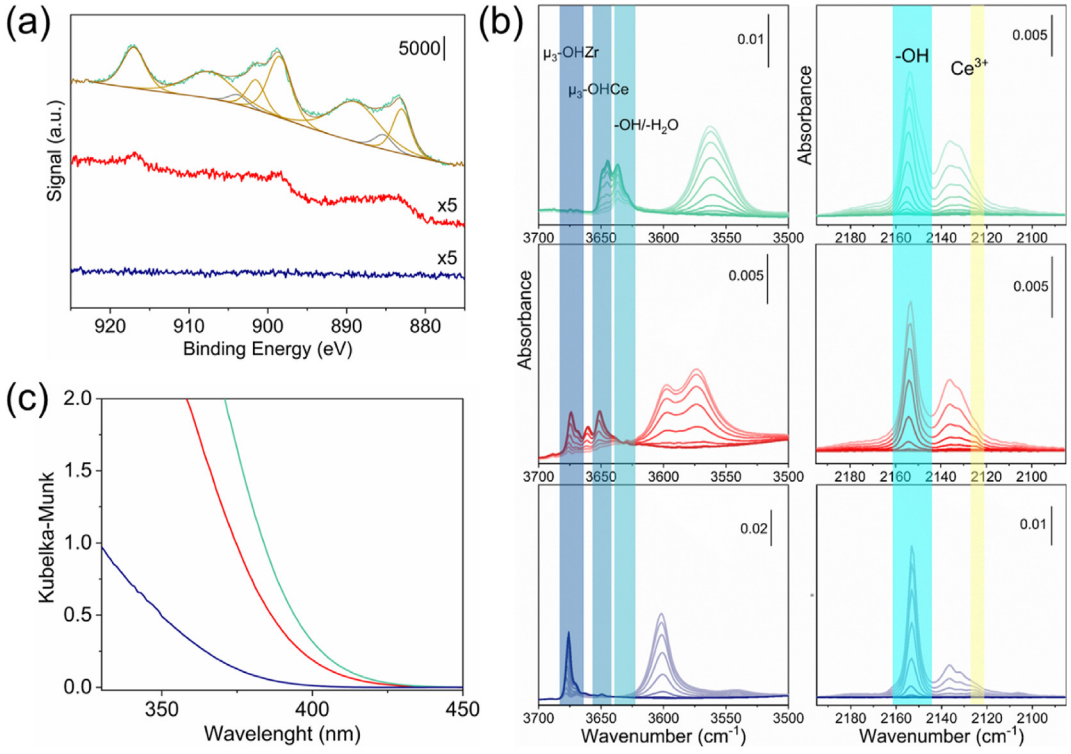

Fig. 6. (a) Ce(3d) XPS spectra, (b) IR spectra of CO desorption at LNT and (c) DR UV-vis spectra of Ce-UiO-66 (green line), $Ce_{0.5}Zr_{0.5}$-UiO-66 (red line) and $Ce_{0.05}Zr_{0.95}$-UiO-66 (blue line). The evolution spectra in CO desorption goes from light to dark lines. Adapted with permission from Ref. [26]. Copyright 2023 Elsevier.

456 cm^{-1} attributed to the F_{2g} vibrational mode of UiO-66(Ce), is shifted to lower wavenumbers (from 456 cm^{-1} to 416 cm^{-1} for CSUST-1) due to the increment of Ce(III)-V_0 abundance as was reported previously by Lu et al. [42]. On the other hand, the EPR signal of CSUST-1 in dark conditions with strong intensity at g = 2.003 is a typical fingerprint of surface Ce(III)-V_0. UV−vis light irradiation causes the spin intensity to increase since CSUST-1 can produce excitons, which can be further separated to give electrons and holes. CSUST-1 was combined with carbon nanotubes (CNTs) to form a CSUST-1/CNT composite to produce a separator coating material for Li−S batteries, by remarkably accelerating the redox kinetics of the polysulfides and the Li^+ transportation. In fact, Li−S cells with the CSUST-1/CNT-coated separator revealed a high initial specific capacity of 1468 mA h/g at 0.1C, and maintained long-term stability for a capacity of 538 mA h/g after 1 200 cycles at 2C, with a decay rate of only 0.037 % per cycle. The interactions between Ce(IV)-MOFs/CNT composites and polysulfides were studied by adding both activated CSUST-1/CNT and UiO-66(Ce)/CNT into the Li_2S_4 electrolyte solution. Ce(IV)-MOFs/CNT composites efficiently adsorbed Li_2S_4 as the solutions became almost colourless. XPS measurements were performed to explore the changes on the surfaces of Ce-MOFs/CNT composites after these adsorption tests, as Fig. 5d displays. The peaks of S $2p^{3/2}$ at 161.7 eV and 163.6 eV are attributed to the terminal S (S_T) and bridging S (S_B), respectively, and the peaks at 167.5 eV and 169.1 eV are due to the formation of surface thiosulfate and polythionate, respectively, which might be generated by the catalytic oxidation of polysulfides induced by the Ce(IV)-MOFs.

3. Hybrid bimetallic M/Ce-MOFs for catalysis

3.1. Pre-formed bimetallic M/Ce-MOFs

CeO_2 and CeO_2-ZrO_2 solid solutions have been commonly employed as catalysts for oxidation reactions [43] and for oxygen storage due to their special redox properties [44]. In fact, Ce(IV) doping in the ZrO_2 matrix has demonstrated an enhancement in the redox properties as a consequence of Ce/Zr ionic radii differences and the generation of oxygen vacancies (Ce(III)-V_0) [34,35]. In this sense, mixed Ce/Zr(IV)-MOFs can allow us to rationalise the position and vicinity of both metals while enhancing the catalytic properties of the subnanometric bimetallic clusters. Since the first synthesis of a Ce-doped Zr(IV)-MOF in 2013 [45], many groups have rationalised and designed a large variety of Ce/Zr-MOFs with different topologies [46–48]. The main goal of such investigations is the improvement of the stability of the Ce(IV)-MOFs, while the redox chemistry of Ce in the subnanometric clusters has not been deeply studied. In our group, we demonstrated by means of XAS and IR spectroscopies that with a Ce doping of less than 10 % in a Zr-UiO-66 matrix, there is a mixture of pure Zr_6-clusters and $CeZr_5$ ones, while with higher concentrations of Ce, pure Ce_6-clusters were also observed [49].

More recently, we studied the redox behaviour of the same Ce-doped Zr(IV)-UiO-66 MOFs by means of handy spectroscopic techniques [26]. When Ce is more diluted in the Zr(IV)-UiO-66 matrix, XPS spectroscopy is not sensitive enough to detect Ce signal (Fig. 6a). However, IR spectroscopy of CO adsorbed at LNT is able to detect accessible Ce(III) species due to the appearance of the band at ~2 125 cm^{-1}, even when Ce is present at low concentrations (Fig. 6b). This was also corroborated by means of UV-vis spectroscopy in which the spectra of the materials are red-shifted upon activation, assigning this tendency to Ce(III) formation and oxygen vacancies increment (Fig. 6c). Even though most of these spectroscopic techniques are really accessible, they have not been commonly employed as tools to unveil the redox behaviour of Ce during catalysis. For example, a successful Ce doping in CAU-24(Zr) (1 Ce atom per Zr_6-cluster) resulted in an enhanced selective catalytic reduction (SCR) of NO with NH_3 [50]. This higher activity is explained by the combination of acidic Zr and redox-active Ce sites to adsorb and oxidise ammonia, respectively. However, even if the acidity of the materials was studied by NH_3 adsorption, the redox behaviour of the Ce(IV)/Ce(III) pair was not unravelled by any spectroscopic technique and its nature remains unclear. In fact, the authors claimed that future papers should be focused on the study of Ce/Zr(IV)-MOFs that allow the formation of oxygen vacancies. In a similar way, Loosen et al. found that the presence of 1 Ce atom per Zr_6-cluster in Ce/Zr-UiO-66 is beneficial for the oxidation of cysteine while the redox behaviour of the Ce(IV)/Ce(III) pair was not studied [51]. More recently, Hou et al. [52] suggested by means of EPR measurements that Ce doping in the Zr-MOF-808 leads to the cleavage of

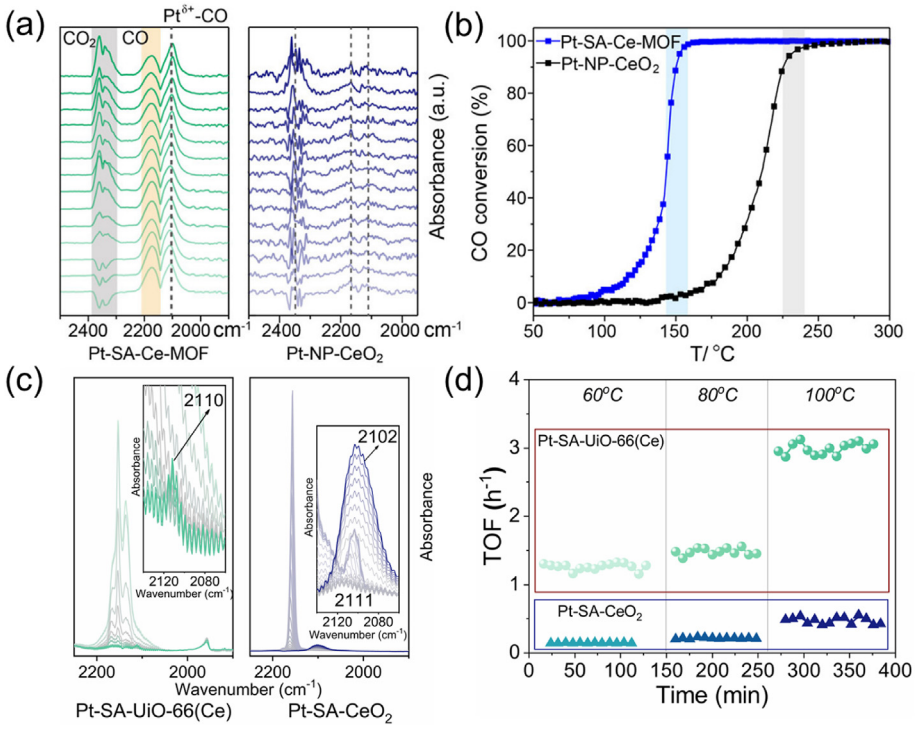

Fig. 7. (a) DRIFT spectra collected during CO oxidation under increasing temperature from 40 °C to 300 °C (from light to dark line) for Pt-SA-Ce-MOF and Pt-NP-CeO_2, respectively the green and blue series; (b) Light-off curves based on CO conversion obtained for both materials; (c) IR spectra of CO adsorbed on Pt-SA-UiO-66(Ce) and Pt-SA-CeO_2 collected during heating (from LNT to RT, from light to dark line). (d) TOF values obtained for the CO oxidation at different temperatures. Adapted with permission from Refs. [59,60]. Copyright 2020 and 2023 American Chemical Society.

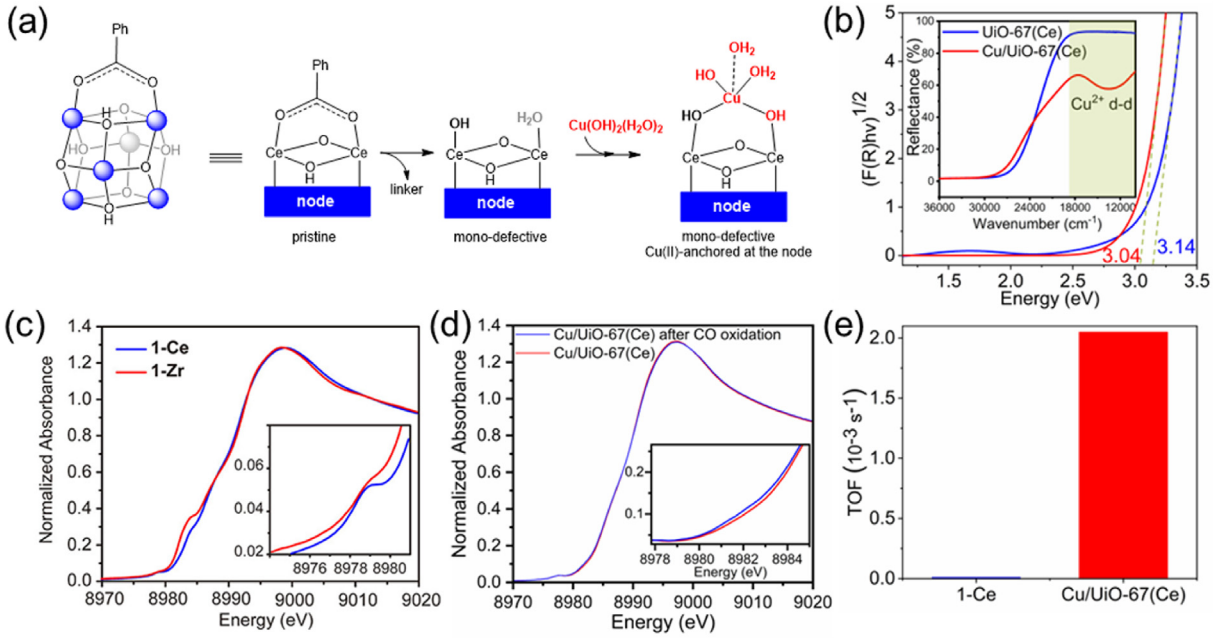

Fig. 8. (a) Cu(II)-incorporation into a defective Ce-node; (b) Tauc plots of the UiO-67(Ce) (blue line) and Cu/UiO-67(Ce) (red line). DR UV-vis spectra of UiO-67(Ce) and Cu/UiO-67(Ce) are reported in the inset; Cu K-edge XANES spectra of (c) Cu/MOF-808(Ce) (hereafter named 1-Ce, blue spectrum) and Cu/MOF-808(Zr) (denoted 1-Zr, red spectrum) and (d) Cu/UiO-67(Ce) before (red spectrum) and after CO oxidation (blue spectrum); (e) TOF values obtained for the CO oxidation at 125 °C using 1-Ce and Cu/UiO-67(Ce) as catalysts. Adapted with permission from Refs. [63,64]. Copyright 2020 and 2024 American Chemical Society.

Zr-O bond and, consequently, oxygen vacancies are generated. Thanks to this spectroscopic technique, the authors found a linear correlation between this oxygen defectivity and the catalytic activity for the toluene oxidation reaction. Moreover, *in situ* diffuse reflectance infra-red Fourier transform (DRIFT) spectroscopy under real reaction conditions was employed to study the reaction intermediates and mechanism for toluene oxidation. Unfortunately, the reported data are not very clear and should be re-considered, reporting them in the appropriate Kubelka-Munk units and paying more attention to the contributions of the vibrational bands of the organic ligands that strongly interfere in the region of interest (the range of 1 400 cm^{-1} to 1 700 cm^{-1}) as they are affected by the presence of the reaction media. In fact, when the spectra collected under real conditions were subtracted to the activated sample, the resulting spectra are very unclear, not allowing any robust band assignment and spectra interpretation.

Apart from the peculiar ability of these hybrid materials in redox catalysis, Ce doping could also enhance the acid-base properties for different organic transformations. For instance, Huo et al. [53] have reported the increase on the number of acidic and medium basic sites with Ce(III) doping in Zr-UiO-66 by means of temperature-programmed desorption of ammonia and carbon dioxide, respectively. Moreover, XPS analysis reveals the incorporation of Ce(III) ions into the Zr_6-clusters, while no characteristic diffraction peaks for Ce 3d appeared on samples with a low cerium content due to the limit of detection of XPS. Finally, and even if this work shows a compressive analysis of the nature of active sites, there is no linear correlation between the amount of these centres and the catalytic activity for dimethyl carbonate (DMC) synthesis from the direct reaction of CO_2 and methanol and the factors affecting catalytic activity remain unclear. In this sense, Bai et al. [54] demonstrated by XPS and UV-vis the coexistence of Ce(IV)/Ce(III) sites and oxygen vacancies in Ce/Zr-UiO-66, respectively. In this case, an enhancement on the catalytic performance for DMC synthesis was also observed with the Ce doping, but it was associated with the increase of the Lewis acidity and not by the redox properties of the hybrid material.

3.2. *Anchored M sites into Ce-clusters*

In the literature panorama, Zr(IV)-MOFs have been extensively employed as supports of metal single sites, clusters and NPs [55–58]. The subnanometric size of the ZrO_x units along the framework permits a control on the position and size of these metallic species which is demonstrated to play a key role for catalysis. More recently, there are on-going studies on Ce(IV)-counterparts as supports, owing to their ability of both Ce(III) sites or oxygen vacancies to stabilise isolated metal sites. However, the role of Ce sites during real reaction conditions remains unclear. For instance, Pt single-atom catalyst supported on a Ce(IV)-MOF, denoted as Pt-SA-Ce-MOF, has exhibited a high activity for the CO oxidation reaction under low temperature conditions [59]. *In situ* Diffuse Reflectance Infrared Fourier Transform (DRIFT) experiments showed that this material interacts with CO molecules even at 40 °C, while a reference material based on Pt NPs supported on CeO_2, named as Pt-NP-CeO_2, showed minimal CO activation in all the temperature-range studied (Fig. 7a). Moreover, the authors claimed that the higher concentration of oxygen vacancies in Pt-SA-Ce-MOF, corroborated by XPS and Raman spectroscopies, could play an important role in the O_2 activation. In fact, these two factors could explain the higher catalytic activity of the material based on Pt single-atom species supported in a Ce-MOF in comparison with the classic Pt-NP-CeO_2 catalyst (Fig. 7b). More recently, our group contributed to this topic, reporting the synthesis of a defective UiO-66(Ce) which is able to stabilise single Pt species [60]. The anchoring of the Pt species has been followed by IR spectroscopy, showing the erosion of specific OH groups upon the Pt functionalization. Moreover, we demonstrated by different spectroscopic techniques, including UV–vis and Ce L_3-edge XANES spectroscopy, the co-presence of oxygen vacancies occupied by Pt single-sites and free oxygen vacancies that are able to activate oxygen molecules during CO oxidation. Finally, IR spectra of CO adsorbed collected during heating from LNT to room temperature showed that the Pt species on the Ce(IV)-MOF support (corresponding to a band centred at 2110 cm^{-1}) are

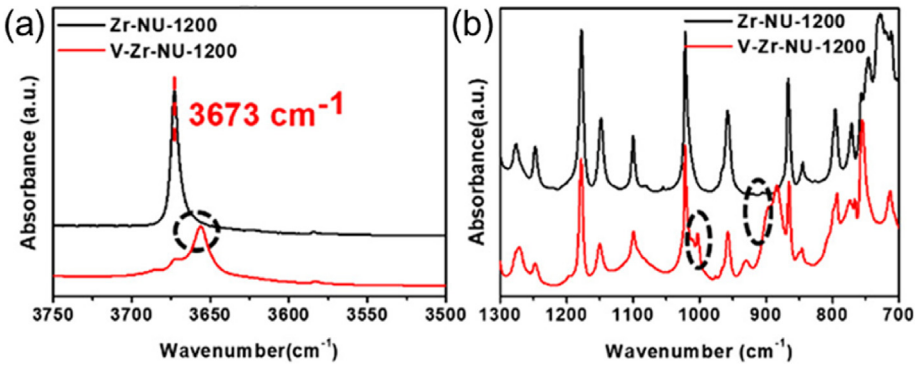

Fig. 9. DRIFT spectra of Zr-NU-1200 and V-Zr-NU-1200 focused on (a) O-H and (b) Zr−O−V vibration regions. Adapted with permission from Ref. [65]. Copyright 2019 American Chemical Society.

more stable than the ones supported on a nanocrystalline cerium oxide, in which the isolated Pt species are reduced by heating (showing a band shift from 2 111 cm^{-1} to 2 102 cm^{-1}) (Fig. 7c). This is translated as an improvement on the catalytic performance for the CO oxidation in comparison with a traditional Pt-SA-CeO_2 catalyst (Fig. 7d).

On the other hand, Ce(IV)-MOFs have been also employed as supports of non-noble metal sites. For instance, Antil et al. [61] have described a heterogeneous catalyst based on Co single-sites supported on the nodes of a UiO-66(Ce) for the partial oxidation of methane to methanol. Elemental analysis showed an incorporation of 1 Co atom per Ce_6-cluster, while XAS and XPS spectroscopies together with DFT calculations revealed the monomeric Co(III) nature of these sites. Interestingly, the Co/UiO-66(Ce) catalyst is at least 10 times more active than Co/UiO-66(Zr) for the oxidation of methane. The author explained this enhancement on the catalytic performance by the highly electron-deficient nature of the cobalt species supported on the Ce_6-nodes, which promotes C−H activation of methane via σ-bond metathesis. In a similar way, Begum et al. synthesised a Ni-based catalyst supported on the Ce/Zr nodes of a UiO-66 structure [62]. Computational and XAS studies reveal that Ni sites are interacting with the μ_3-OH group of the bimetallic clusters and, concretely, with that which is directly bonded with the Ce atom. Furthermore, XPS analysis suggested the presence of Ni(II) ions while Ce is almost presented as Ce(IV). However, the deconvoluted XPS spectra were not supporting the experimental ones since the Ce(III) component is missing, ruling out the possible redox effect of Ce as support and during catalysis. Cu-based species have been also anchored into the hexanuclear clusters of different Ce(IV)-MOFs. For example, Román-Leshkov et al. reported the synthesis of non-noble isolated Cu species supported on the Ce_6-based clusters of MOF-808(Ce) (Fig. 8a) [63]. This synthetic method consists on a solvothermal process in which $Cu(OAc)_2{\cdot}H_2O$ was employed as a metal source. ICP measurement suggested the incorporation of 4 Cu atoms per Ce_6-cluster, while XAS analysis revealed the Cu(II) nature and its presence as a mononuclear site (Fig. 8b). Conversely, Cu(II) species supported on MOF-808(Zr) are in the form of multinuclear sites, which has a direct correlation for catalysis: concretely, it is translated in a higher catalytic activity of the Ce(IV)-based support in comparison with the Zr(IV) one for CO and cyclohexane oxidation reactions. Even if the results presented on these works are promising from a catalytic point of view, the redox behaviour of Ce during real reaction conditions and its effect during catalysis remain unclear. Recently, our group reported the synthesis of a UiO-67(Ce), which promotes the anchoring of dispersed Cu(II) sites through Ce_6-clusters (Fig. 8a) [64]. Both TGA analysis and IR spectra of CO adsorbed demonstrated the presence of defective Ce(IV) sites that can promote the Cu incorporation. Moreover, XAS and UV-vis measurements revealed Cu species in their initial state as isolated Cu(II) (Figs. 8b to d). However, during the catalytic CO

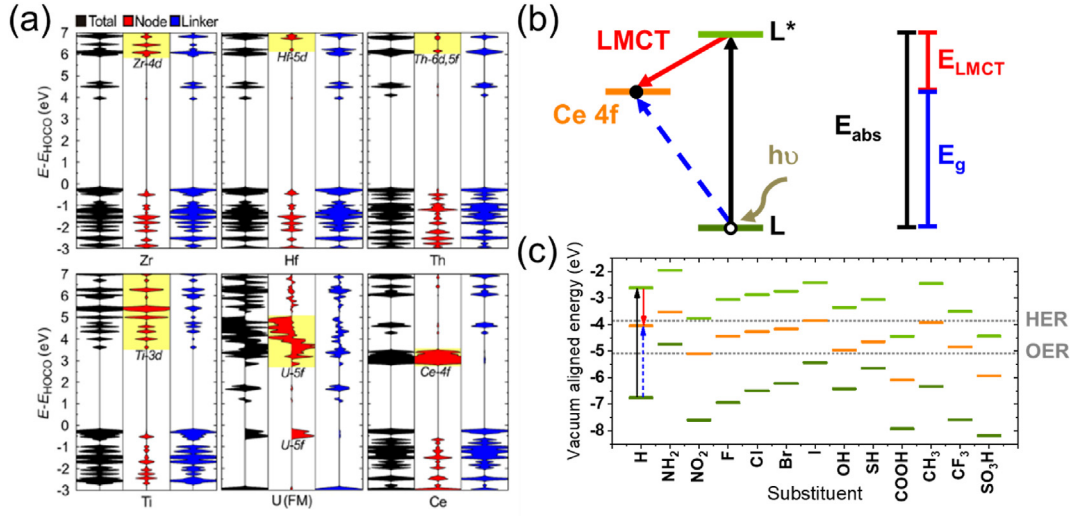

Fig. 10. (a) Total (black), metal-(blue) and ligand-projected (red) density of states from DFT for various M-UiO-66 with M(IV) = Zr, Hf, Th, Ti, U (in ferromagnetic spin configuration), and Ce(IV); (b) Schematic representation of the photoelectron generation and charge-separation process on a Ce(IV)-MOF; (c) Representation of the key energy levels (vacuum aligned) of variously linker-monosubstituted Ce-UiO-66: linker ground state (dark green), linker excited state (light green) and Ce *4f* states (orange). Redox potentials for HER and OER reactions are highlighted by grey dotted lines. Adapted with permission from Ref. [67]. Copyright 2018 American Chemical Society.

oxidation, these sites are reduced to Cu(I) ones (Fig. 8d), which is translated into an improvement on the catalytic performance. *In situ* and *operando* IR and XAS spectroscopies revealed the co-presence of Cu(I) and Ce(III) sites which is beneficial for catalysis, since CO molecules could be adsorbed onto Cu(I) sites and react with the O_2 molecules activated closed to the Ce(III) sites, closing the catalytic cycle in a synergic fashion. This is translated into a higher catalytic activity of the Cu/UiO-67(Ce) in comparison to the Cu/MOF-808(Ce), as shown in Fig. 8e.

Finally, this Ce redox behaviour might also not be beneficial for catalytic purposes. For instance, Farha et al. have reported the synthesis of vanadium catalyst supported on different isostructural M-NU-1200 (with M = Zr, Hf, Ce and Th) [65]. DRIFT spectrum of activated Zr-NU-1200 shows a band at 3 673 cm^{-1} associated with μ_3-OH groups of the metallic cluster (see black spectrum in Fig. 9a). The consumption of this component together with the appearance of a new feature at lower wavenumbers after vanadium incorporation indicate that V is directly bonded to the nodes (see red spectrum in Fig. 9a). Moreover, this fact could be corroborated by the presence of a band at 900 cm^{-1} that can be assigned to V−O−Zr vibration (Fig. 9b). Finally, the V-based catalyst supported on the nodes of Zr-NU-1200 demonstrated the highest activity for the oxidation of 4-methoxybenzyl alcohol. Post-catalytic XPS and EPR analyses on the material showed that V sites were reduced from V(V) to V(IV) during the oxidation reaction. The lowest activity, obtained for the V-Ce-NU-1200, is ascribed to the only presence of V(V) sites that remain after catalysis. This could be related to *in situ* re-oxidation of V(IV) sites favoured by the reduction of Ce(IV) to Ce(III) sites.

4. Ce(IV)-MOFs for photocatalysis

Besides applications in thermal catalysis, photo-catalytic processes involving MOFs are attracting a noticeable interest in the community in recent years. [66]. In this context, spectroscopies (in particular optical spectroscopy and photoluminescence spectroscopy) are primary tools to achieve a thorough understanding of the electronic structure of the potential photocatalysts. Moreover, their coupling with computational methods offers considerable advantages at obtaining a precise atomistic description of the involved electronic processes. Ce(IV)-MOFs raised particular attention in the field, as dictated by their peculiar electronic structure inferred by the combination of an organic moiety (the ligand) with Ce(IV)-based clusters, thanks to their conveniently energy-localised *4f* states. In fact, as almost simultaneously reported by Wu et al. [67] and Hendrickx et al. [68] for the prototype UiO-66 framework, Ce(IV)-based materials feature empty *4f* states lying at lower energy with respect to excited states of the linker. This electronic configuration, unattainable with other UiO-66 forming metals (Fig. 10a), makes possible the charge-separation that is vital for supporting any photochemical process, as schematized in Fig. 10b.

In brief, the incoming photons with energy $h\nu \geq E_{abs}$ (Fig. 10b) are primarily absorbed by the linker, featuring a high absorption coefficient as expected from the type of involved transition (generally a π-π^*). The electron can subsequently decay from the excited π^* state to the empty Ce *4f* orbitals, via a negative ligand-to-metal charge transfer (LMCT) with energy E_{LMCT}: in this way, the electron is spatially displaced from the linker and its recombination with the hole in the ground state is delayed, making photocatalytic processes feasible from the electronic perspective. On the other side, a direct excitation from the linker ground state to the Ce *4f* states by a photon with energy $h\nu \geq E_g$ (Fig. 10b), even though possible as experimentally demonstrated, has an intrinsically poor cross section, then is not of primary interest for the charge-separation process. According to the scheme in Fig. 10b, minimising E_{abs} is desirable in order to increase the photon harvesting capability of Ce-UiO-66. As a matter of fact, the terephthalate ligands absorb in the UV region, and a shift toward the visible is mandatory in the view of real applications. This goal can be achieved with appropriate molecular engineering of the linker, *i.e.*, by functionalizing it with opportune groups. As an example, the insertion of a -NH_2 group significantly shifts the linker absorption toward the visible, roughly yielding a red-shift of E_{abs} of 1.4 eV. However, the increased light harvesting via E_{abs} decrease is not sufficient to provide an enhanced photoactivity. An important parameter to be considered is, in fact, the correct alignment of the energy levels with respect to the redox potentials for the targeted photoreactions. As an example, to perform an electron-driven photoreduction, the final state of the photoexcited electron (*i.e.*, the Ce *4f* states) must lie at an energy higher than the potential for the targeted reaction. This translates in the requirement of a sufficiently large E_g to overcome the aforementioned redox potential. The same consideration stands for oxidation reactions promoted by holes, as the energetic ground state of the linker should fall below the associated potential to occur. Taking as a paradigmatic example the photocatalytic water splitting reaction and its half-reactions (the oxygen evolution reaction, OER, and the hydrogen evolution reaction, HER), depending on the electronic structure of the photocatalyst it may be possible to perform both the half-reaction simultaneously or, possibly, only one of them (Fig. 10c). In the case of Ce-UiO-66-NH_2, for instance, the relatively small values of E_{abs} and E_{LMCT} make this material optimal for the application in the HER under the electronic point of view, whereas its energy of the ground state is too high, hampering its usage for the OER. Many substituted linkers are theoretically suitable for the OER, in particular -I and -SH substitution.

Beside these fundamental investigations, several literature contributions dealt with practical application of Ce(IV)-MOFs to photocatalytic reactions. In a recent study Garcia, Serre and co-workers [69] demonstrated the feasibility of water splitting half-reactions (as well as of the overall process) under sun-like illumination over Ce-UiO-66 with opportune linker modification. The authors identified Ce-UiO-66-NH_2 and Ce-UiO-66-NO_2, respectively, as the best HER and OER photocatalysts in their samples series. Furthermore, they showed the feasibility of overall water splitting on Ce-UiO-66-NH_2, greatly enhanced by the inclusion of Pt nanoparticles as co-catalyst. Nonetheless, gas evolution rates remain quite limited (in the order of few tens μmol/g evolved per hour) and the photoreaction rate decreases along irradiation time (suggesting a progressive deactivation of the catalyst). Other research efforts towards water splitting over Ce(IV)-MOFs included the modification of the metal cluster with dopants to finely tune the electronic properties of the Ce *4f* states [70,71], as well as the *ex novo* design of new structures featuring extensively π-conjugated linkers [72,73]. Both strategies revealed their effectiveness in boosting photocatalytic properties towards water splitting, and we foresee more and more contributions will deal with fine tuning of electronic and structural properties of Ce(IV)-MOFs in the following years.

Apart from water splitting, another common application field of Ce(IV)-MOFs as photocatalysts is either complete or partial oxidation reactions. The former type is commonly adopted in the field of environmental remediation, where the abatement of organic pollutants is achieved via their complete oxidation to CO_2. Several literature examples discuss the performances of Ce(IV)-MOFs toward the abatement of model pollutants, such as formaldehyde [73] or phenol [71], but rarely provide extensive characterization of materials, in particular during operation. Partial photo-oxidation reactions offer more room towards the assessment of the oxidation mechanism and the structure-properties relation of the investigated system, since the MOF topology can significantly affect the selectivity alongside its electronic properties. As an example, Campanelli et al. [74] studied the effect of linker substitution and topology of Ce(IV)-MOFs in the selective oxidation of para-substituted benzyl alcohols. They highlighted the dominant role of incorporating electron withdrawing groups in the linker (*i.e.*, -NO_2 or -Br substitution, or even replacement of terephthalic acid by the pyridine-2,5 dicarboxylic one) in enhancing the hole-electron pair lifetime, with a positive effect on the yield in the desired product. Another very interesting study by Ji et al. [75] is focussed on the aerobic oxidation of saturated alkanes to the corresponding ketones photocatalyzed by a novel Ce-based MOF featuring mixed valence Ce(IV)/Ce(III) in combination with anthraquinone-2,7-dicarboxylic acid as linker. This material, named Ce-AQ, was specifically engineered to mimic the reactivity of the

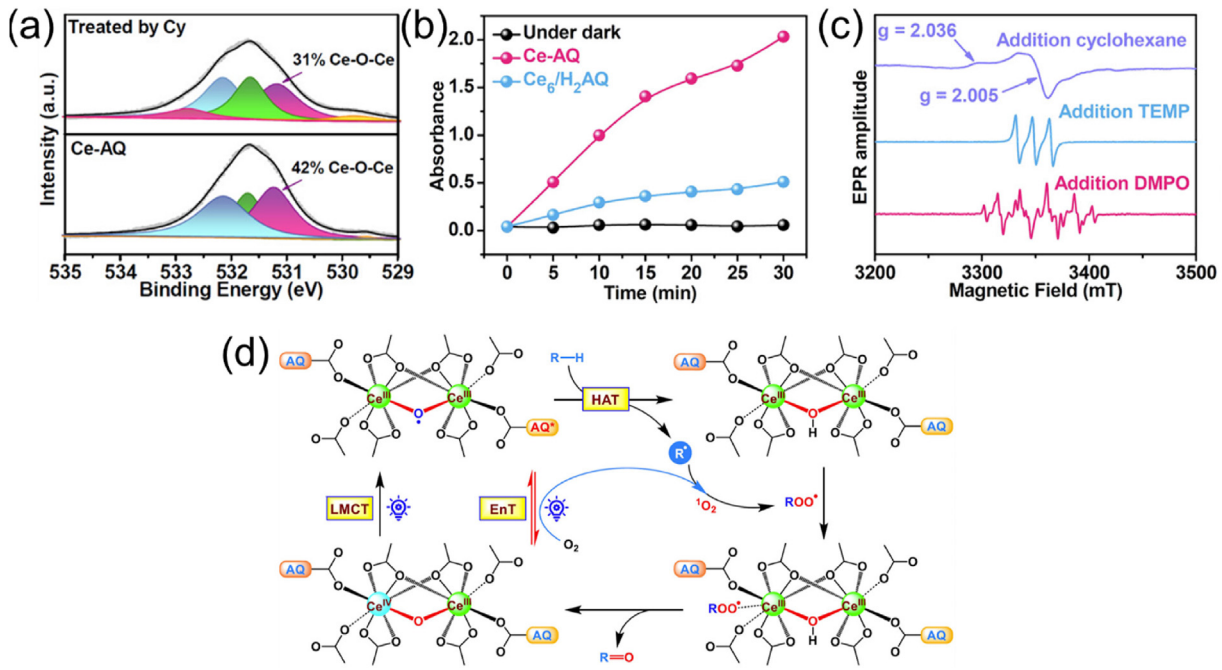

Fig. 11. (a) Ce3d XPS spectra of Ce-AQ as such and contacted with cyclohexane; (b) Photometric TMP oxidation essay on Ce-AQ and hexanuclear Ce-based clusters/linker mixture; (c) EPR spectra of ROSs trapped by the substrate and other trapping molecules; (d) Hypothetical reaction mechanism for cycloalkanes selective oxygenation to the corresponding ketones, based on spectroscopic evidence. Adapted with permission from Ref. [75]. Copyright 2022 American Chemical Society.

binuclear iron monooxygenase enzyme and showed excellent performances in the selective oxygenation of cyclohexane and other cycloalkanes to the corresponding ketones. The complex radical mechanism of the reaction was thoroughly investigated by combining several methodologies, including spectroscopic approaches. By investigating the interaction of cyclohexane with Ce-AQ via Ce3d XPS (Fig. 11a), the authors assessed as the alkane can interact directly with a Ce(III)-O-Ce(IV) bridge along the one-dimensional inorganic building unit, by forming a weak hydrogen bond through one of its H atoms. Indeed, the component associated with the Ce(III)-O-Ce(IV) moiety in the spectrum decreases in intensity, while the linewidth of the Ce3d signal overall increases. The structure of this adsorbate was further determined by single-crystal XRD of cyclohexane-soaked Ce-AQ. Beside the capability of adsorbing the substrate, the generation of reactive oxygen species (ROSs) by Ce-AQ was determined by a spectroscopic approach (Fig. 11b) based on the oxidation of tetramethylbenzidine (TMB), a chromogenic substrate commonly used in enzymology to track peroxidase activity. In presence of illumination ($\lambda = 395$ nm), Ce-AQ triggers a significant production of ROSs, as monitored by the increase of the absorbance of TMB oxidative products observing their electronic transition at 400 nm. Their rate of formation is much higher for Ce-AQ than for a mixture of the anthraquinone-2,7-dicarboxylic acid linker with hexanuclear Ce(IV)-based clusters, highlighting the synergistic effect of the inorganic building unit and the organic linker in photogenerating the ROSs. Such ROSs were further qualified by means of a combination of EPR spectroscopy (Fig. 11c, also taking advantage of trapping molecules) and assay reactions (*i.e.*, terpinene oxidation). The EPR spectra collected under illumination in presence of 2,2,6,6-tetramethylpiperidine (TEMP) and 5,5-dimethyl-1-pyrroline N-oxide (DMPO) allowed identifying singlet oxygen ($^1O_2$) and the superoxide radical anion ($O_2^{\bullet-}$) as the main ROSs, being the former the most abundant according to the preferential conversion of terpinene in ascaridole in an assay reaction. Furthermore, the interaction of cyclohexene with Ce-AQ under illumination produced an EPR signal the author interpreted as due to the formation of cyclohexyl and cyclohexyl peroxyl radicals, suggesting that a H atom from the substrate has been extracted by the MOF, likely by a Ce(III)-O-Ce(IV) bridge. Merging all these pieces of information, a reaction mechanism has been proposed (Fig. 11d). At first, the photoinduced LMCT transition promotes the formation of oxygen bridge radicals along the Ce(III)-O-Ce(IV) inorganic chains, capable of activating the C–H bond in the substrate via abstraction of the H atom. Simultaneously, the anthraquinone linkers act as active sites for the generation of reactive oxygen species, namely singlet oxygen. The reaction of the latter with the organic radicals generated by H-transfer produces secondary radicals that, by further interacting with the MOF are quenched with the simultaneous restoring of the pristine Ce(III)-O-Ce(IV) sites, by eliminating the reaction products (mainly ketones).

5. Summary and perspectives

The interest towards Ce-MOFs is increasing in the scientific community thanks to their versatility in many areas associated with catalytic phenomena and the larger accessibility of Ce precursors. Moreover, if compared to other tetravalent-based MOFs (both Hf and Zr), it is possible to benefit from their redox activity retaining good thermal and chemical stabilities that overall characterize tetravalent-based MOFs. In general the materials under study in this perspective review are modified versions of Ce(IV)-based MOFs for both thermocatalytic and photocatalytic applications. A large platform of experimental and theoretical approaches are available to allow a detailed characterization of these materials at any stage of the preparation and often also under reaction conditions: a multi-technique assessment is advisable for an in depth understanding of behaviors of the materials allowing to attempt structure-performance correlations. Despite the availability of the techniques, the execution and the interpretation of the experiments are not always coherent. Moreover, none of these approaches can be used "alone" and more robust conclusions can be achieved when many techniques are used in parallel adopting very similar conditions and on the same, consistent and homogeneous set of samples: in particular, this is a general rule of thumb, not only valid in the specific case of Ce(IV)-based MOFs.

Moreover, several aspects should be contemplated prior to the individual utilization of these characterization techniques keeping in mind the intrinsic limit of any technique. In this sense, standard XPS

spectroscopy has been commonly employed to determine the oxidation state of Ce at the surface, even if the extreme high *vacuo* of the measuring chamber easily causes the partial reduction of Ce during the measurement falsifying the result. Conversely, XAS spectroscopy applicable at the K, L and M edges offers an alternative to unveil the average oxidation state of Ce-MOF samples, but the poor accessibility of the technique, which generally requires access to synchrotron beamlines, limits its routine use.

As recently reported, CO adsorption monitored by IR spectroscopy can corroborate the presence of Ce(III) sites while also determining its accessibility. However, even if IR spectroscopy of probe molecules is a powerful technique to study the nature of active sites and reaction intermediates, its use and the analysis of the results should be considered in a correct way. Finally, in a period where fast characterization methods are needed, UV-vis spectroscopy offers an easy way to determine the presence of reduced Ce sites on Ce(IV)-MOFs. These considerations have a general value and extend to all characterization techniques (not only spectroscopic) when applied to study the behavior of Ce-MOFs in (photo) catalysis.

Declaration of competing interest

The authors declare no conflict of interest.

Acknowledgements

The authors acknowledge the funding from Horizon 2020 Excellence Science ERC-Synergy program 2019-CUBE: “Unravelling the secrets of Cu-based catalysts for C–H activation” (Grant No. 856446) and from the Project CH4.0 under the MUR Program “Dipartimenti di Eccellenza 2023–2027" (CUPD13C22003520001). Valeria Finelli's activities have been conducted during and with the support of the Italian national inter-university PhD course in Sustainable Development and Climate change (PhD-SDC). Sergio Rojas-Buzo acknowledges the Margarita Salas grant financed by the Ministerio de Universidades, Spain, and also funded by the European Union-Next Generation EU.

References

[1] A. Corma, H.I. Garcia, F.X. Llabrés i Xamena, Engineering metal organic frameworks for heterogeneous catalysis, Chem. Rev. 110 (2010) 4606–4655, https://doi.org/10.1021/cr9003924.
[2] A.H. Chughtai, N. Ahmad, H.A. Younus, A. Laypkov, F. Verpoort, Metal–organic frameworks: versatile heterogeneous catalysts for efficient catalytic organic transformations, Chem. Soc. Rev. 44 (2015) 6804–6849, https://doi.org/10.1039/C4CS00395K.
[3] A. Bavykina, N. Kolobov, I.S. Khan, J.A. Bau, A. Ramirez, J. Gascon, Metal–organic frameworks in heterogeneous catalysis: recent progress, new trends, and future perspectives, Chem. Rev. 120 (2020) 8468–8535, https://doi.org/10.1021/acs.chemrev.9b00685.
[4] J.H. Cavka, S. Jakobsen, U. Olsbye, N. Guillou, C. Lamberti, S. Bordiga, K.P. Lillerud, A new zirconium inorganic building brick forming metal organic frameworks with exceptional stability, J. Am. Chem. Soc. 130 (2008) 13850–13851, https://doi.org/10.1021/ja8057953.
[5] Y. Bai, Y. Dou, L.-H. Xie, W. Rutledge, J.-R. Li, H.-C. Zhou, Zr-based metal–organic frameworks: design, synthesis, structure, and applications, Chem. Soc. Rev. 45 (2016) 2327–2367, https://doi.org/10.1039/C5CS00837A.
[6] P. García-García, A. Corma, Hf-based metal-organic frameworks in heterogeneous catalysis, Isr. J. Chem. 58 (2018) 1062–1074, https://doi.org/10.1002/ijch.201800099.
[7] Z. Hu, Y. Wang, D. Zhao, The chemistry and applications of hafnium and cerium (IV) metal–organic frameworks, Chem. Soc. Rev. 50 (2021) 4629–4683, https://doi.org/10.1039/D0CS00920B.
[8] J. Jacobsen, A. Ienco, R. D'Amato, F. Costantino, N. Stock, The chemistry of Ce-based metal–organic frameworks, Dalton Trans. 49 (2020) 16551–16586, https://doi.org/10.1039/D0DT02813D.
[9] M. Lammert, M.T. Wharmby, S. Smolders, B. Bueken, A. Lieb, K.A. Lomachenko, D. De Vos, N. Stock, Cerium-based metal organic frameworks with UiO-66 architecture: synthesis, properties and redox catalytic activity, Chem. Commun. 51 (2015) 12578–12581, https://doi.org/10.1039/C5CC02606G.
[10] M. Lammert, C. Glißmann, H. Reinsch, N. Stock, Synthesis and characterization of new Ce(IV)-MOFs exhibiting various framework topologies, Cryst. Growth Des. 17 (2017) 1125–1131, https://doi.org/10.1021/acs.cgd.6b01512.
[11] T.E. Webber, S.P. Desai, R.L. Combs, S. Bingham, C.C. Lu, R.L. Penn, Size control of the MOF NU-1000 through manipulation of the modulator/linker competition, Cryst. Growth Des. 20 (2020) 2965–2972, https://doi.org/10.1021/acs.cgd.9b01590.
[12] V. Finelli, G. Mastronardi, N.G. Porcaro, M. Signorile, F. Bonino, P.A. Szilagyi, S. Bordiga, Synthesis of mixed-linker Ce-UiO-67 metal-organic framework, RSC Appl. Interfaces (2024), https://doi.org/10.1039/D4LF00278D. Accepted Manuscript.
[13] J. Jacobsen, L. Wegner, H. Reinsch, N. Stock, Ce-MIL-140: expanding the synthesis routes for cerium(IV) metal–organic frameworks, Dalton Trans. 49 (2020) 11396–11402, https://doi.org/10.1039/D0DT02455D.
[14] C. Lamberti, A. Zecchina, E. Groppo, S. Bordiga, Probing the surfaces of heterogeneous catalysts by in situ IR spectroscopy, Chem. Soc. Rev. 39 (2010) 4951–5001, https://doi.org/10.1039/C0CS00117A.
[15] J.G. Vitillo, T. Lescouet, M. Savonnet, D. Farrusseng, S. Bordiga, Soft synthesis of isocyanate-functionalised metal–organic frameworks, Dalton Trans. 41 (2012) 14236–14238, https://doi.org/10.1039/C2DT31977B.
[16] F. Bonino, C. Lamberti, S. Bordiga, IR and Raman Spectroscopies Probing MOFs Structure, Defectivity, and Reactivity, Wiley Online Library, 2016, https://doi.org/10.1002/9783527693078.ch22.
[17] F. Bonino, C. Lamberti, S. Chavan, J.G. Vitillo, S. Bordiga, Characterization of MOFs. 1. Combined vibrational and electronic spectroscopies, in: F. Llabres i Xamena, J. Gascon (Eds.), Metal Organic Frameworks as Heterogeneous Catalysts, The Royal Society of Chemistry, 2013, pp. 76–142, https://doi.org/10.1039/9781849737586-00076.
[18] F. Nouar, M.I. Breeze, B.C. Campo, A. Vimont, G. Clet, M. Daturi, T. Devic, R.I. Walton, C. Serre, Tuning the properties of the UiO-66 metal organic framework by Ce substitution, Chem. Commun. 51 (2015) 14458–14461, https://doi.org/10.1039/C5CC05072C.
[19] T. Barzetti, E. Selli, D. Moscotti, L. Forni, Pyridine and ammonia as probes for FTIR analysis of solid acid catalysts, Faraday Trans. 92 (1996) 1401–1407, https://doi.org/10.1039/FT9969201401.
[20] E. Groppo, S. Rojas-Buzo, S. Bordiga, The role of in situ/operando IR spectroscopy in unraveling adsorbate-induced structural changes in heterogeneous catalysis, Chem. Rev. 123 (2023) 12135–12169, https://doi.org/10.1021/acs.chemrev.3c00372.
[21] K.I. Hadjiivanov, G.N. Vayssilov, Characterization of oxide surfaces and zeolites by carbon monoxide as an IR probe molecule, Adv. Catal. 47 (2002) 307–511, https://doi.org/10.1016/S0360-0564(02)47008-3.
[22] C. Morterra, G. Magnacca, A case study: surface chemistry and surface structure of catalytic aluminas, as studied by vibrational spectroscopy of adsorbed species, Catal. Today 27 (1996) 497–532, https://doi.org/10.1016/0920-5861(95)00163-8.
[23] H. Leclerc, A. Vimont, J.-C. Lavalley, M. Daturi, A.D. Wiersum, P.L. Llwellyn, P. Horcajada, G. Férey, C. Serre, Infrared study of the influence of reducible iron (III) metal sites on the adsorption of CO, CO 2, propane, propene and propyne in the mesoporous metal–organic framework MIL-100, Phys. Chem. Chem. Phys. 13 (2011) 11748–11756, https://doi.org/10.1039/C1CP20502A.
[24] C. Atzori, K.A. Lomachenko, J. Jacobsen, N. Stock, A. Damin, F. Bonino, S. Bordiga, Bimetallic hexanuclear clusters in Ce/Zr-UiO-66 MOFs: in situ FTIR spectroscopy and modelling insights, Dalton Trans. 49 (2020) 5794–5797, https://doi.org/10.1039/D0DT01023E.
[25] S. Rojas-Buzo, P. Concepción, J.L. Olloqui-Sariego, M. Moliner, A. Corma, Metalloenzyme-inspired Ce-MOF catalyst for oxidative halogenation reactions, ACS Appl. Mater. Interfaces 13 (2021) 31021–31030, https://doi.org/10.1021/acsami.1c07496.
[26] S. Rojas-Buzo, D. Salusso, F. Bonino, M.C. Paganini, S. Bordiga, Unraveling the reversible formation of defective Ce3+ sites in the UiO-66 (Ce) material: a multi-technique study, Mater. Today Chem. 27 (2023) 101337, https://doi.org/10.1016/j.mtchem.2022.101337.
[27] E. Cerrato, C. Gionco, M.C. Paganini, E. Giamello, E. Albanese, G. Pacchioni, Origin of visible light photoactivity of the CeO2/ZnO heterojunction, ACS Appl. Energy Mater. 1 (2018) 4247–4260, https://doi.org/10.1021/acsaem.8b00887.
[28] C. Gionco, E. Giamello, L. Mino, M.C. Paganini, The interaction of oxygen with the surface of CeO 2–TiO 2 mixed systems: an example of fully reversible surface-to-molecule electron transfer, Phys. Chem. Chem. Phys. 16 (2014) 21438–21445, https://doi.org/10.1039/C4CP03195D.
[29] S. Livraghi, M.C. Paganini, E. Giamello, G. Di Liberto, S. Tosoni, G. Pacchioni, Formation of reversible adducts by adsorption of oxygen on Ce–ZrO2: an unusual η2 ionic superoxide, J. Phys. Chem. C 123 (2019) 27088–27096, https://doi.org/10.1021/acs.jpcc.9b08615.
[30] E. Paparazzo, Corrigendum: use and mis-use of x-ray photoemission Ce3d spectra of Ce2O3 and CeO2, Phys. Condens. Matter 32 (2020) 099501, https://doi.org/10.1088/1361-648X/ab5763.
[31] S. Bordiga, F. Bonino, K.P. Lillerud, C. Lamberti, X-ray absorption spectroscopies: useful tools to understand metallorganic frameworks structure and reactivity, Chem. Soc. Rev. 39 (2010) 4885–4927, https://doi.org/10.1039/C0CS00082E.
[32] P. Nachimuthu, W.-C. Shih, R.-S. Liu, L.-Y. Jang, J.-M. Chen, The study of nanocrystalline cerium oxide by X-ray absorption spectroscopy, J. Solid State Chem. 149 (2000) 408–413, https://doi.org/10.1006/jssc.1999.8566.
[33] A.M. Shahin, F. Grandjean, G.J. Long, T.P. Schuman, Cerium LIII-edge XAS investigation of the structure of crystalline and amorphous cerium oxides, Chem. Mater. 17 (2005) 315–321, https://doi.org/10.1021/cm0492437.
[34] D. Salusso, S. Mauri, G. Deplano, P. Torelli, S. Bordiga, S. Rojas-Buzo, MOF-derived CeO2 and CeZrOx solid solutions: exploring Ce reduction through FTIR and

NEXAFS spectroscopy, Nanomaterials 13 (2023) 272, https://doi.org/10.3390/nano13020272.
[35] S. Rojas-Buzo, D. Salusso, A. Jouve, E. Bracciotti, M. Signorile, S. Bordiga, CO2 to dimethylcarbonate synthesis: surface defects and oxygen vacancies engineering on MOF-derived CexZr1− xO2− y catalysts, Appl. Catal., B: Environment and Energy 346 (2024) 123723, https://doi.org/10.1016/j.apcatb.2024.123723.
[36] L. Chu, J. Guo, Z. Huang, H. Yang, M. Yang, G. Wang, Excellent catalytic performance over acid-treated MOF-808(Ce) for oxidative desulfurization of dibenzothiophene, Fuel 332 (2023) 126012, https://doi.org/10.1016/j.fuel.2022.126012.
[37] C. Volkringer, H. Leclerc, J.-C. Lavalley, T. Loiseau, G. Férey, M. Daturi, A. Vimont, Infrared spectroscopy investigation of the acid sites in the metal–organic framework aluminum trimesate MIL-100(Al), J. Phys. Chem. C 116 (2012) 5710–5719, https://doi.org/10.1021/jp210671t.
[38] R. Dalapati, B. Sakthivel, M.K. Ghosalya, A. Dhakshinamoorthy, S. Biswas, A cerium-based metal–organic framework having inherent oxidase-like activity applicable for colorimetric sensing of biothiols and aerobic oxidation of thiols, CrystEngComm 19 (2017) 5915–5925, https://doi.org/10.1039/C7CE01053B.
[39] S. Smolders, K.A. Lomachenko, B. Bueken, A. Struyf, A.L. Bugaev, C. Atzori, N. Stock, C. Lamberti, M.B.J. Roeffaers, D.E. De Vos, Unravelling the redox-catalytic behavior of Ce4+ metal–organic frameworks by X-ray absorption spectroscopy, ChemPhysChem 19 (2018) 373–378, https://doi.org/10.1002/cphc.201700967.
[40] Y. Zhang, X. Zeng, X. Jiang, H. Chen, Z. Long, Ce-based UiO-66 metal-organic frameworks as a new redox catalyst for atomic spectrometric determination of Se(VI) and colorimetric sensing of Hg(II), Microchem. J. 149 (2019) 103967, https://doi.org/10.1016/j.microc.2019.103967.
[41] H.-G. Jin, M. Wang, J.-X. Wen, S.-H. Han, X.-J. Hong, Y.-P. Cai, G. Li, J. Fan, Z.-S. Chao, Oxygen vacancy-rich mixed-valence cerium MOF: an efficient separator coating to high-performance lithium–sulfur batteries, ACS Appl. Mater. Interfaces 13 (2021) 3899–3910, https://doi.org/10.1021/acsami.0c18899.
[42] G.-P. Lu, X. Li, L. Zhong, S. Li, F. Chen, Ru@UiO-66(Ce) catalyzed acceptorless dehydrogenation of primary amines to nitriles: the roles of Lewis acid–base pairs in the reaction, Green Chem. 21 (2019) 5386–5393, https://doi.org/10.1039/C9GC02181G.
[43] P. Fang, M.-F. Luo, J.-Q. Lu, S.-Q. Cen, X.-Y. Yan, X.-X. Wang, Studies on the oxidation properties of nanopowder CeO2-based solid solution catalysts for model soot combustion, Thermochim. Acta 478 (2008) 45–50, https://doi.org/10.1016/j.tca.2008.08.017.
[44] C.E. Hori, H. Permana, K.Y.S. Ng, A. Brenner, K. More, K.M. Rahmoeller, D. Belton, Thermal stability of oxygen storage properties in a mixed CeO2-ZrO2 system, Appl. Catal., B 16 (1998) 105–117, https://doi.org/10.1016/S0926-3373(97)00060-X.
[45] A.M. Ebrahim, T.J. Bandosz, Ce(III) doped Zr-based MOFs as excellent NO2 adsorbents at ambient conditions, ACS Appl. Mater. Interfaces 5 (2013) 10565–10573, https://doi.org/10.1021/am402305u.
[46] Y. Zhai, Y. Li, Q. Hou, Y. Zhang, E. Zhou, H. Li, S. Ai, Highly sensitive colorimetric detection and effective adsorption of phosphate based on MOF-808(Zr/Ce), New J. Chem. 46 (2022) 15405–15413, https://doi.org/10.1039/D2NJ00640E.
[47] X. Dong, Y. Lin, Y. Ma, L. Zhao, Ce-doped UiO-67 nanocrystals with improved adsorption property for removal of organic dyes, RSC Adv. 9 (2019) 27674–27683, https://doi.org/10.1039/C9RA05586J.
[48] M. Lammert, C. Glißmann, N. Stock, Tuning the stability of bimetallic Ce(iv)/Zr(iv)-based MOFs with UiO-66 and MOF-808 structures, Dalton Trans. 46 (2017) 2425–2429, https://doi.org/10.1039/C7DT00259A.
[49] K.A. Lomachenko, J. Jacobsen, A.L. Bugaev, C. Atzori, F. Bonino, S. Bordiga, N. Stock, C. Lamberti, Exact stoichiometry of CexZr6–x cornerstones in mixed-metal UiO-66 metal–organic frameworks revealed by extended X-ray absorption fine structure spectroscopy, J. Am. Chem. Soc. 140 (2018) 17379–17383, https://doi.org/10.1021/jacs.8b10343.
[50] S. Smolders, J. Jacobsen, N. Stock, D. De Vos, Selective catalytic reduction of NO by cerium-based metal–organic frameworks, Catal. Sci. Technol. 10 (2020) 337–341, https://doi.org/10.1039/C9CY02029B.
[51] A. Loosen, C. Simms, S. Smolders, D.E. De Vos, T.N. Parac-Vogt, Bimetallic Ce/Zr UiO-66 metal–organic framework nanostructures as peptidase and oxidase nanozymes, ACS Appl. Nano Mater. 4 (2021) 5748–5757, https://doi.org/10.1021/acsanm.1c00546.
[52] X. Hou, L. Jin, C. Wang, L. Gu, J. Li, L. Yang, Non-noble metal-doped MOF-808-Zr nanostructures with abundant defects for toluene oxidation, ACS Appl. Nano Mater. 6 (2023) 17397–17405, https://doi.org/10.1021/acsanm.3c02198.
[53] L. Huo, L. Wang, J. Li, Y. Pu, K. Xuan, C. Qiao, H. Yang, Cerium doped Zr-based metal-organic framework as catalyst for direct synthesis of dimethyl carbonate from CO2 and methanol, J. CO2 Util. 68 (2023) 102352, https://doi.org/10.1016/j.jcou.2022.102352.
[54] J. Bai, Z. Song, L. Liu, X. Zhu, F. Gao, R.V. Chaudhari, Enhanced transformation of CO2 over microporous Ce-doped Zr metal–organic frameworks, RSC Adv. 12 (2022) 26307–26318, https://doi.org/10.1039/D2RA02680E.
[55] T. Ikuno, J. Zheng, A. Vjunov, M. Sanchez-Sanchez, M.A. Ortuño, D.R. Pahls, J.L. Fulton, D.M. Camaioni, Z. Li, D. Ray, Methane oxidation to methanol catalyzed by Cu-oxo clusters stabilized in NU-1000 metal–organic framework, J. Am. Chem. Soc. 139 (2017) 10294–10301, https://doi.org/10.1021/jacs.7b02936.
[56] J. Zheng, J. Ye, M.A. Ortuño, J.L. Fulton, O.Y. Gutiérrez, D.M. Camaioni, R.K. Motkuri, Z. Li, T.E. Webber, B.L. Mehdi, Selective methane oxidation to methanol on Cu-oxo dimers stabilized by zirconia nodes of an NU-1000 metal–organic framework, J. Am. Chem. Soc. 141 (2019) 9292–9304, https://doi.org/10.1021/jacs.9b02902.
[57] Y. Yang, X. Zhang, S. Kanchanakungwankul, Z. Lu, H. Noh, Z.H. Syed, O.K. Farha, D.G. Truhlar, J.T. Hupp, Unexpected "spontaneous" evolution of catalytic, MOF-supported single Cu (II) cations to catalytic, MOF-supported Cu (0) nanoparticles, J. Am. Chem. Soc. 142 (2020) 21169–21177, https://doi.org/10.1021/jacs.0c10367.
[58] G. Fang, F. Wei, J. Lin, Y. Zhou, L. Sun, X. Shang, S. Lin, X. Wang, Retrofitting Zr-Oxo nodes of UiO-66 by Ru single atoms to boost methane hydroxylation with nearly total selectivity, J. Am. Chem. Soc. 145 (2023) 13169–13180, https://doi.org/10.1021/jacs.3c02121.
[59] S. Guo, Y. Zhao, C. Wang, H. Jiang, G.J. Cheng, A single-atomic noble metal enclosed defective MOF via cryogenic UV photoreduction for CO oxidation with ultrahigh efficiency and stability, ACS Appl. Mater. Interfaces 12 (2020) 26068–26075, https://doi.org/10.1021/acsami.0c06898.
[60] S. Rojas-Buzo, B. Bohigues, D. Salusso, A. Corma, M. Moliner, S. Bordiga, Synergic effect of isolated Ce3+ and Ptδ+ species in UiO-66(Ce) for heterogeneous catalysis, ACS Catal. 13 (2023) 9171–9180, https://doi.org/10.1021/acscatal.3c00502.
[61] N. Antil, M. Chauhan, N. Akhtar, R. Newar, W. Begum, J. Malik, K. Manna, Metal–organic framework-encaged monomeric cobalt(III) hydroperoxides enable chemoselective methane oxidation to methanol, ACS Catal. 12 (2022) 11159–11168, https://doi.org/10.1021/acscatal.2c02823.
[62] W. Begum, M. Chauhan, R. Kalita, P. Gupta, N. Akhtar, N. Antil, R. Newar, K. Manna, Synergetic Ni–Ce active sites in mixed cerium/zirconium metal–organic framework nodes for selective methane oxidation into ethanol, ACS Catal. 14 (2024) 10427–10436, https://doi.org/10.1021/acscatal.4c02883.
[63] X. He, B.G. Looker, K.T. Dinh, A.W. Stubbs, T. Chen, R.J. Meyer, P. Serna, Y. Román-Leshkov, K.M. Lancaster, M. Dincă, Cerium(IV) enhances the catalytic oxidation activity of single-site Cu active sites in MOFs, ACS Catal. 10 (2020) 7820–7825, https://doi.org/10.1021/acscatal.0c02493.
[64] S. Rojas-Buzo, D. Salusso, T.-H.T. Le, M.A. Ortuño, K.A. Lomachenko, S. Bordiga, Unveiling the role and stabilization mechanism of Cu+ into defective Ce-MOF clusters during CO oxidation, J. Phys. Chem. Lett. 15 (2024) 3962–3967, https://doi.org/10.1021/acs.jpclett.4c00324.
[65] X. Wang, X. Zhang, P. Li, K. Otake, Y. Cui, J. Lyu, M.D. Krzyaniak, Y. Zhang, Z. Li, J. Liu, C.T. Buru, T. Islamoglu, M.R. Wasielewski, Z. Li, O.K. Farha, Vanadium catalyst on isostructural transition metal, lanthanide, and actinide based metal–organic frameworks for alcohol oxidation, J. Am. Chem. Soc. 141 (2019) 8306–8314, https://doi.org/10.1021/jacs.9b02603.
[66] a) W. Han, L.-H. Shao, X.-J. Sun, Y.-H. Liu, F.-M. Zhang, Y. Wang, P.-Y. Dong, G.-L. Zhang, Constructing Cu ion sites in MOF/COF heterostructure for noble-metal-free photoredox catalysis, Appl. Catal. B Environ. 317 (2022) 121710, https://doi.org/10.1016/j.apcatb.2022.121710;
b) P. Dong, J. Pan, L. Zhang, X.-Li Yang, M.-H. Xie, J. Zhang, Regulation of electron delocalization between flower-like (Co, Ni)-MOF array and WO3/W photoanode for effective photoelectrochemical water splitting, Appl. Catal., B: Environment and Energy 350 (2024) 123925, https://doi.org/10.1016/j.apcatb.2024.123925;
c) P. Dong, K. Gao, L. Zhang, H. Huan, M.-H. Xie, X.-L. Yang, J. Zhang, Hydrogen bond-assisted construction of MOF/semiconductor heterojunction photocatalysts for highly efficient electron transfer, Appl. Catal., B: Environment and Energy 357 (2024) 124297, https://doi.org/10.1016/j.apcatb.2024.124297.
[67] X.-P. Wu, L. Gagliardi, D.G. Truhlar, Cerium metal–organic framework for photocatalysis, J. Am. Chem. Soc. 140 (2018) 7904–7912, https://doi.org/10.1021/jacs.8b03613.
[68] K. Hendrickx, J.J. Joos, A. De Vos, D. Poelman, P.F. Smet, V. Van Speybroeck, P. Van Der Voort, K. Lejaeghere, Exploring lanthanide doping in UiO-66: a combined experimental and computational study of the electronic structure, Inorg. Chem. 57 (2018) 5463–5474, https://doi.org/10.1021/acs.inorgchem.8b00425.
[69] S. Dai, E. Montero-Lanzuela, A. Tissot, H.G. Baldoví, H. García, S. Navalón, C. Serre, Room temperature design of Ce(iv)-MOFs: from photocatalytic HER and OER to overall water splitting under simulated sunlight irradiation, Chem. Sci. 14 (2023) 3451–3461, https://doi.org/10.1039/D2SC05161C.
[70] M.A. Syzgantseva, C.P. Ireland, F.M. Ebrahim, B. Smit, O.A. Syzgantseva, Metal substitution as the method of modifying electronic structure of metal–organic frameworks, J. Am. Chem. Soc. 141 (2019) 6271–6278, https://doi.org/10.1021/jacs.8b13667.
[71] P. Parnicka, W. Lisowski, T. Klimczuk, A. Mikolajczyk, A. Zaleska-Medynska, A novel (Ti/Ce)UiO-X MOFs@TiO2 heterojunction for enhanced photocatalytic performance: boosting via Ce4+/Ce3+ and Ti4+/Ti3+ redox mediators, Appl. Catal., B 310 (2022) 121349, https://doi.org/10.1016/j.apcatb.2022.121349.
[72] J.-X. Gu, H. Chen, Y. Ren, Z.-G. Gu, G. Li, W.-J. Xu, X.-Y. Yang, J.-X. Wen, J.-T. Wu, H.-G. Jin, A novel cerium(IV)-Based metal-organic framework for CO2 chemical fixation and photocatalytic overall water splitting, ChemSusChem 15 (2022) e202102368, https://doi.org/10.1002/cssc.202102368.
[73] H. Yang, L. Jia, Z. Zhang, B. Xu, Z. Liu, Q. Zhang, Y. Cao, Z. Nan, M. Zhang, T. Ohno, Novel cerium-based MOFs photocatalyst for photocarrier collaborative performance under visible light, J. Catal. 405 (2022) 74–83, https://doi.org/10.1016/j.jcat.2021.11.017.
[74] M. Campanelli, T. Del Giacco, F. De Angelis, E. Mosconi, M. Taddei, F. Marmottini, R. D'Amato, F. Costantino, Solvent-free synthetic route for cerium(IV) metal–organic frameworks with UiO-66 architecture and their photocatalytic applications, ACS Appl. Mater. Interfaces 11 (2019) 45031–45037, https://doi.org/10.1021/acsami.9b13730.
[75] G. Ji, L. Zhao, Y. Wang, Y. Tang, C. He, S. Liu, C. Duan, A binuclear cerium-based metal–organic framework as an artificial monooxygenase for the saturated hydrocarbon aerobic oxidation with high efficiency and high selectivity, ACS Catal. 12 (2022) 7821–7832, https://doi.org/10.1021/acscatal.2c01030.